Proceedings World Geothermal Congress 2020+1
Reykjavik, Iceland, April - October 2021

Probabilistic Approach for 3D Conceptual Modelling Using Multi Geophysical Data

Hisako Mochinaga[1], Naoshi Aoki[1], David Sunwall[2], Michael S. Zhdanov[2] and Takuji Mouri[3]

1: JGI, Inc., 1-5-21, Otsuka, Bunkyo-ku, Tokyo 1130012, Japan

2: TechnoImaging LLC, Suite 500, 4001 South, 700 East, Salt Lake City UT 84107, USA

3: Japan Oil, Gas and Metals National Corporation, 2-10-1, Toranomon, Minato-ku, Tokyo 1050001, Japan

E-mail: hisako.mochinaga@jgi.co.jp

Keywords: 3D Conceptual Modelling, Artificial Neural Networks, Seismic Attributes, Bayesian Classification.

ABSTRACT

Production sustainability of geothermal resources requires accurate and high definition conceptual model focusing on temperature and permeability. Probabilistic approach facilitates investigation and analysis of complex subsurface structures regarding geothermal reservoirs, cap rocks, recharge areas and faults associated with hydrothermal system. In this paper, we present a case study of 3D conceptual modelling at the Onikobe geothermal field in northeast Japan. There has been multimodal dataset consisted of surface seismic, magnetotelluric (MT), airborne gravity gradiometry (AGG) and gravity surveys in addition to borehole data. These geophysical data provide subsurface structures regarding rock properties to interpret hydrothermal system. Especially, surface seismic data have valuable information on not only velocity structure, but also fault and fracture images represented by geometric attributes that are automatically extracted such as Thinned Fault Likelihood (Hale, 2013), dip azimuth, and curvature attributes (Roberts, 2001). Thus, the geometric attributes are significant to understand spatial distributions of fault-controlled geothermal reservoirs. These seismic attributes and rock properties can be quantitatively integrated by means of multi-attribute analysis (MAA). We have implemented a probabilistic MAA that with the artificial neural network (ANN) algorithm developed by Hampson et al. (2001) for a cost-effective solution of the non-linear problem in geothermal modelling. In this workflow, the probabilistic approach makes it possible to provide a detailed geothermal model while taking advantage of higher spatial resolution of 3D surface seismic data. Another probabilistic approach, Bayesian classification, is a robust tool for permeability assessment in the conceptual modelling. We performed Bayesian classification based on non-parametric probability density functions (PDFs) using resistivity, P-wave impedance and Thinned Fault Likelihood attribute. The comprehensive interpretation from the detailed litho-facies model is consistent with the observed distributions of temperature, permeability and hydrothermal fluids beneath the Onikobe caldera. It reveals that the probabilistic conceptual modelling yields significant benefits for geothermal exploration and exploitation.

1. INTRODUCTION

After the Great East Japan Earthquake struck in 2011, the government of Japan has been encouraging us to the growth of the total installed capacity in supplying electricity from renewable resources. As a part of the campaigns, Japan Oil, Gas and Metals National Corporation (JOGMEC) undertook geothermal exploration demonstration projects to better understand hydrothermal systems using advanced airborne measurements and 3D surface seismic data. Application of 3D seismic technology is aiming at the development of techniques for higher-resolution geothermal reservoir visualization. The first demonstration field was planned on flat land which is close to the Yamagawa geothermal power station (Fukuda et al., 2016, Endo et al., 2018). In contrast with the first field, the second demonstration field was deployed within the Onikobe caldera in mountainous volcanic area located in northeast Japan (Mouri et al, 2019).

In the past, New Energy and Industrial Technology Development Organization (NEDO) had undertaken exploration and appraisal drilling campaigns for researching the geothermal resources in Kurikoma area including the Onikobe caldera from 1980 to 1988 (e.g. NEDO, 1985;1988). During the large-scale project, many geological and geophysical surveys were done to estimate subsurface structures for the exploration of geothermal resources. As for reconnaissance, gravity and magnetic exploration methods in potential fields were used in probing the large-scale sub-surface structures generated by volcanic eruption and caldera collapse. Whereas electromagnetic and electrical surveys were particularly appropriate for resistivity structure estimation to delineate heat flow paths in the hydrothermal system. Besides, MT survey had an advantage in regional long-period measurement for probing deeper resistivity structure regarding to the hydrothermal system in the Onikobe caldera. On the other hand, seismic survey had been known as expensive tool for applying in geothermal exploration. Thus, cost-effective 2D seismic survey was much more common for the purpose of fault imaging than 3D seismic survey. There were totally 13 lines of 2D seismic surveys acquired from 1968 to 1969 and from 1982 to1983 in the field.

However, the JOGMEC demonstration projects have proved the advantages of 3D surface seismic data for comprehensive interpretation using multi geophysical data. The new 3D surface seismic data greatly contributes to the improvement of geothermal reservoir visualization due to much higher spatial resolution than others. In this study, we will demonstrate a cost-effective workflow of geophysical and geological integrated analyses in order to improve chance of success in production drilling. The data integration allows us to make a high definition conceptual model focusing on temperature and permeability. Consequently, it will be expected to reduce drilling costs, which are allotted to approximately 30% of total project capital expenditure in domestic geothermal industry.

2. REGIONAL GEOLOGY

2.1 Onikobe Caldera

Onikobe caldera is one of the calderas located on the volcanic front of northeast Japan arc. Many active geysers and hot springs are found within the caldera basin neighboring active volcanos of Mt Kurikoma and Naruko region. The significant characteristics of

geologic structures are caldera collapse, pyroclastic flow plateau and lava domes inside the basin. The major diameter of the sub-circular basin is approximately 10 km and the minor diameter is approximately 8 km. Geological surveys have revealed that the volcanic eruptions were mainly active in Middle Pleistocene. Abe (1985) reported that NW-SE faults were dominant in the area close to the Onikobe geothermal power station. As shown in Figure 1, Cretaceous basement granitic rocks are exposure at ground located at the southeast caldera rim. In addition to the basin structure, the characteristic of shallow structure is a layered structure formed by lacustrine deposits and volcanic debris of andesite lava and tuff, in which some regional faults are aligned in W-E trends. Furthermore, there is the Onikobe-Yuzawa mylonite zone consisted of Cretaceous tonalite and granodiorite in NNW-SSE direction. These features are significant structures to understand the tectonic history of the caldera.

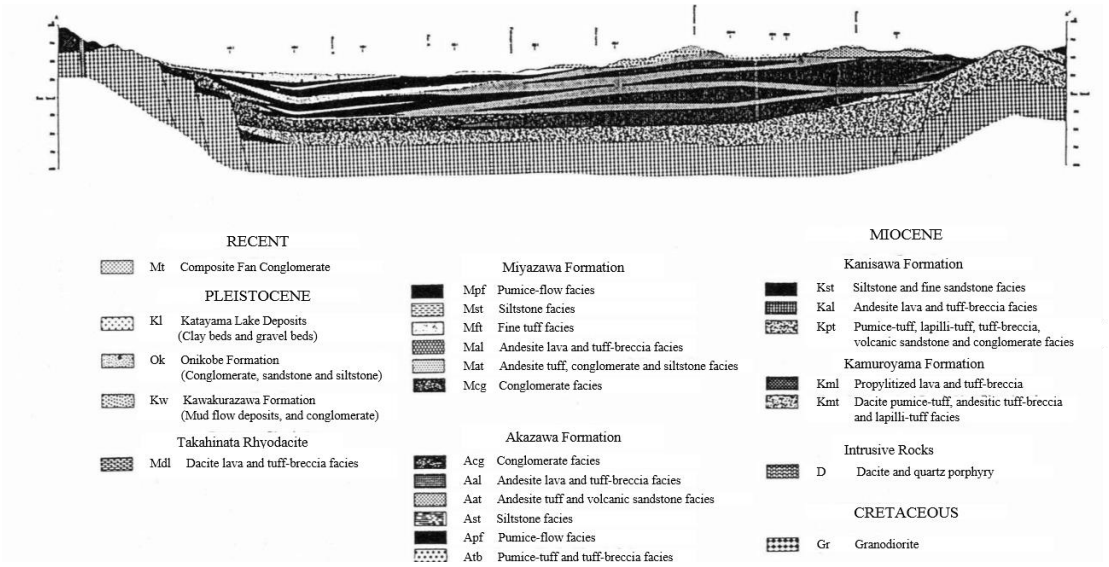

Figure 1: Geologic cross section of the Onikobe caldera in SW-NE direction (After Yamada and Sakaguchi, 1983).

2.2 Geothermal System

Electric Power Development Co., Ltd. (J-Power) had been supplying electricity at the single-flash steam turbine plant, whose installed capacity was 12.5 MW since 1985. The reservoir temperature is approximately over 230˚C. The complicated hydrothermal system has been revealed from geological and geophysical surveys in extensive region at Kurikoma area (NEDO, 1988). For example, geothermal reservoir compartmentalization has been pointed out from production history. Nakanishi (2010) reported that the declines of pressure and temperature indicated the presence of impermeable formation between shallow and deep reservoirs below the power station. The geochemical investigation confirmed the fact of separate spatial distributions of acid fluids, neutral or alkaline fluids below the power station. The shallow reservoirs are saturated with neutral or alkaline fluids. The scale buildups include smectite clay minerals in which is stable under in-situ temperature is less than approximately 150˚C. On the other hand, the deep reservoirs are from hydrothermal fluids with open fractures in pyrophyllite. These open fractures are saturated with acid fluids whose pH value is approximately 3. The presence of massive pyrophyllite indicates hydrothermal alteration under the situation where in-situ temperature is higher than 150˚C. These altered rocks are distributed in areas at approximately 1,000 m below mean sea level (MSL). In this case, to reduce the effects on the reservoir temperature and pressure, optimal well paths have extended from the power station to south and east areas for hot water re-injection, while those of neutral or alkaline fluid production have extended to west area.

3. WORKFLOW

This paper presents a workflow to make an accurate and high-definition conceptual model focusing on temperature and permeability in the geothermal field. Figure 2 shows the workflow diagram to predict the temperature and other rock property models using geophysical and borehole data. The multiple data integration is important to fulfill the primary objective of comprehensive conceptual modelling. A final temperature model is predicted by multi-attribute analysis called MAA (Hampson et al., 2001). As an example of MAA application, Mochinaga et al., (2017) presented an advanced 3D geothermal modelling by means of machine learning with combinations of linear regression and ANN for predicting vertical and lateral heat transfer, respectively. In the Onikobe demonstration project, we applied this prediction approach for the 3D temperature modelling. The other three rock properties of resistivity, P-wave impedance and TFL attribute are utilized for Bayesian classification to build a high-definition conceptual model. These models are ranging from the ground surface to 3,000 m below MSL in depth domain. Each cell size is set to 10 m (inline) x 10 m (crossline) x 5 m (z) as the input data in the MAA process based on seismic and borehole logging data. Almost all models are estimated in depth domain. However, geometric seismic attributes are extracted in time domain due to the sensitivity of analyses. These seismic attributes are finally converted to depth models prior to perform the MAA process.

For an estimation of 3D resistivity structure, several resistivity contour maps, which were compiled by J-Power, have compensated for its limited data availability in this study. We performed three-dimensional interpolation using these contour maps in the same way as an initial temperature model. On the other hand, parameters of density, P-wave and P-wave impedance are given by forward modelling and inversion using the recorded data in potential field and elastic wavefield, respectively. For example, AGG and gravity data is jointly inverted to give an accurate 3D density model. This inverted density model can be used as input data for not only temperature modelling in the MAA process but also P-wave impedance modelling. Besides, refraction tomography provides an inverted low frequency P-wave model using arrival times of refracted waves from each subsurface impedance boundary. This inversion is much more robust method of P-wave velocity structure when probing complex geology compared to use the reflection

data. However, it has a disadvantage regarding its limited ray path coverage. This workflow is designed to overcome these disadvantages on both reflection and refraction data acquired in the mountainous volcanic field. The final P-wave impedance model is inverted from reflection data. As a starting model of this iterative seismic inversion, a low-frequency P-wave impedance model is given by the product of the density model inverted from AGG and gravity data, and the P-wave model based on refraction tomography.

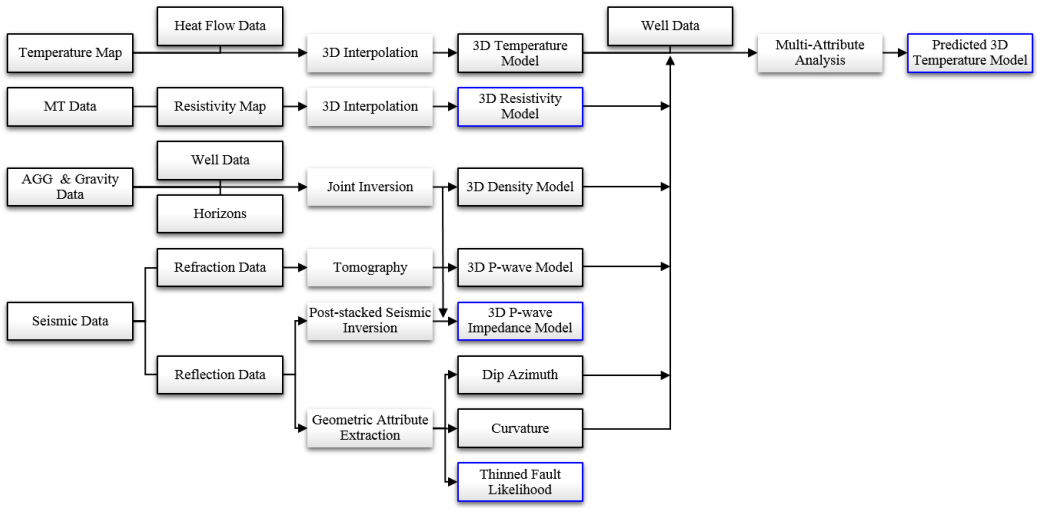

Figure 2: Workflow diagram of multiple data integration. Litho-facies classification is based on 3D rock property models that are displayed in blue.

4. DATA

4.1 Temperature Data

In this workflow, it is necessary to construct a priori low-frequency temperature model for predicting a final accurate and high-definition temperature model. Available dataset consists of temperature logging data, measurements of temperature recovery tests and temperature contour maps compiled by J-power. One is the temperature map measured at 1 m depth from the ground. The other maps are estimated at the MSL, the 250 m above MSL, the 500 m below MSL, the 1,000 m below MSL and the 2,000 m below MSL. The spatial interpolation using the sparse sampled data requires vertical constrains given by a couple of temperature logging data at exploration well locations. Figure 3 shows a 3D view of the interpolated and smoothed temperature model. The grid cell size is set to small enough for fitting to seismic data analysis. Consequently, the interpolated model has a high uncertainty due to the sparse temperature data. In this case, there may be not enough information to discuss drilling optimization. As mentioned, MAA is a useful method to improve accuracy and resolution of an estimated model using both borehole data with higher vertical resolution and seismic data with higher spatial resolution. The details of input data applied for the MAA will be described in the following sections.

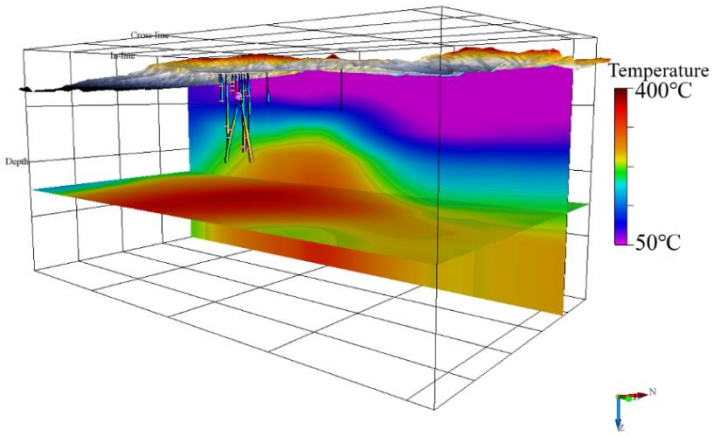

Figure 3: A priori temperature model created by 3D interpolation using temperature contour maps. The top surface indicates topography.

4.2 MT Data

Resistivity is one of the most important rock properties which have been related to temperature. In fact, MT survey has been a popular geophysical survey to understand large-scale resistivity structure in geothermal fields, Japan. NEDO (1985) had done the MT survey at 67 stations that were deployed in the Onikobe basin. Ogawa et al. (1988) estimated resistivity structures by 1D and 2D inversions using the responses of apparent resistivity and phase in both transverse magnetic (TM) mode and transverse electric (TE) mode. For each mode, ten frequency bands were analyzed from 0.02 Hz to 90 Hz. As a result, these vertical profiles explicitly showed characteristics such as high resistivity structure associated with granitic basement and low resistivity structure with locations of faults and distributions of cap rocks and heat sources. However, lacustrine deposits also created low resistivity anomalies in the basin. Thus, it may give a rise to uncertainty in the geothermal reservoir delineation based on only resistivity structures. In the situation, data integration will effectively work to visualize the complex geothermal reservoir in the Onikobe field.

As for the workflow, we have constructed 3D resistivity model by means of 3D interpolation approach as well as temperature model as described in Section 4.1. There are resistivity maps at 500m, 1,000 m and 2,000 m below MSL in addition to the ground surface resistivity map. The 3D gridding and interpolation processes provide a smoothed resistivity model as mentioned before. Figure 4 shows the 3D resistivity model and interpreted faults. In the model, the low resistivity zones are distributed below the power station and along faults extending to western part of the caldera rim. For a validation of the interpolated resistivity model, we examined the reliability using geometric seismic attributes as described in Section 4.4.3.

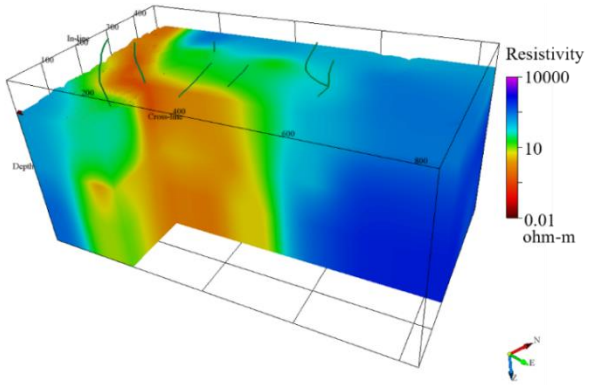

Figure 4: A priori resistivity model created by 3D interpolation using resistivity contour maps from MT data. Green lines indicate interpreted faults from geological surveys.

4.3 AGG and Gravity Data

JOGMEC has been probing widely for prospecting geothermal potentials using AGG measurement system in Japan since 2013. We utilized the AGG and vertical gravity data around the Onikobe caldera for estimating 3D density model. Figure 5 (left) shows the flight lines and it includes total 294,140 data observed at 42,020 stations. These data had been directly measured by the Falcon® measurement system providing six tensor components of gravity gradiometry denoted by G_{xx}, G_{xy}, G_{xz}, G_{yy}, G_{yz} and G_{zz}, including a component of vertical gravity G_z. In general, gravity data are more sensitive to horizontal variation than vertical variation in density structures. However, as mentioned before, the upper layered structure is a significant characteristic of the Onikobe basin. The layered structure may disturb interpretation to gravity anomalies caused by vertical variation in gravity data related to the caldera structure. To overcome the problem, Cai and Zhdanov (2015) have developed a 3D forward modelling method using Cauchy-type integral equation called as depth-to-basement inversion. The inversion algorithm allows us to improve vertical sensitivity as well as horizontal sensitivity. We also applied the joint inversion algorithm with Gramian constraints between AGG and vertical gravity data (Zhdanov, 2015). The horizontal grid size is 100 m (E-W) x 100 m (N-S). The vertical grid size is ranging from 75 m to 175 m with that increasing logarithmically. The inversion process is guided by a priori model that is constrained by the surfaces of topography and basement interpreted from borehole information. In this two-layered model, the upper and lower layers are set to -0.1 g/cm^3 and +0.1 g/cm^3 from the average density model, respectively. Figure 5 (right) shows a 3D view of the jointly inverted relative density model. The feature of the caldera rim has been successfully extracted as well as the details of inner structures. A rectangular shows the area of interest in conceptual modelling according to the coverage of surface seismic survey area.

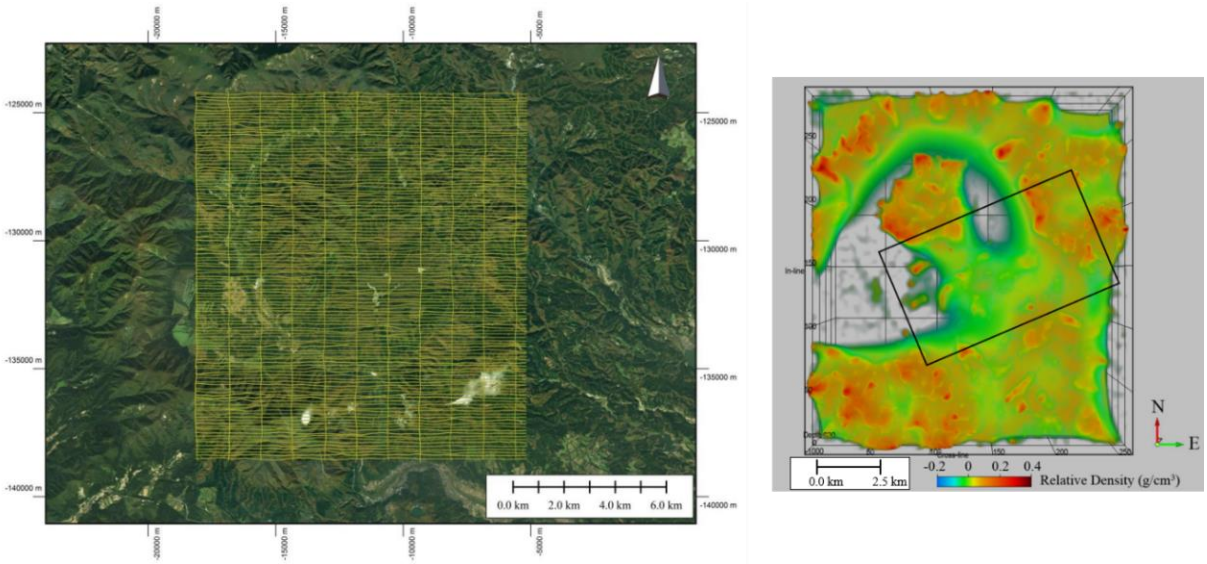

Figure 5: (Left) AGG survey layout. Yellow line denotes flight line. (Right) The jointly inverted relative density volume. Transparent area indicates that the relative density value is lower than -0.1 g/cm^3. Rectangle indicates the target area for conceptual modelling.

4.4 Seismic Data

4.4.1 Seismic Survey

3D seismic data acquisition was mainly done for seismic reflection imaging to the geothermal reservoir visualization in 2017. Figure 6 shows seismic survey layout map in which area covers approximately 35 square kilometers. The irregular deployment of source and receiver locations is one of the characteristics in seismic data acquisition in mountainous volcanic area. As a matter of course, national park regulations and road widths are important to be in consideration for planning survey layout. Besides, hydrothermal altered rocks cause a significant effect on coupling between these sensors and ground formation. Practically, several types of sources and receiver equipment were installed to effectively overcome these drawbacks in the seismic data acquisition. In addition to these considerations in data acquisition, we must devise an appropriate workflow of data processing as means to noise reduction in reflection imaging on volcanic rocks and complex structures in the Onikobe basin. However, heterogeneity in volcanic rock properties generally tends to reduce reflectivity contrasts. Hence it had been thought that it was difficult to imaging volcanic rocks associated with geothermal reservoirs. In this study, seismic inversion and attribute extraction allowed us to perform quantitative interpretation for an accurate and high definition conceptual model using refraction and reflection data.

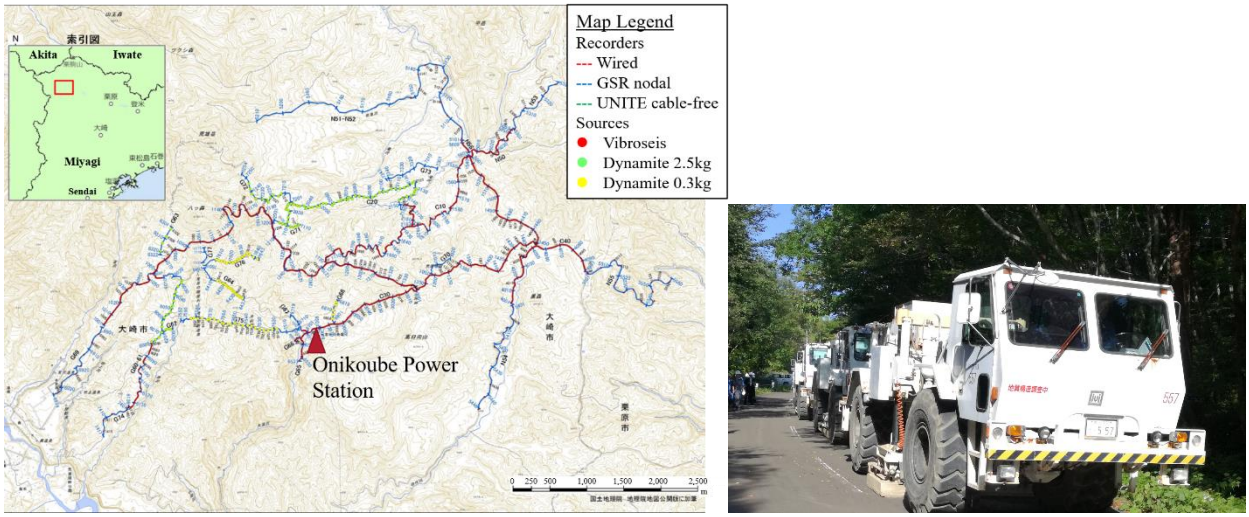

Figure 6: 3D Seismic survey in the demonstration field. (Left) Acquisition layout on the topography map which was published by Geospatial Information Authority of Japan. (Right) A photo of Vibroseis trucks.

4.4.2 Seismic Inversion

Seismic inversion has been used as a common technique to estimate P-wave impedance structure using seismic reflection data. P-wave impedance is defined by product of bulk density and P-wave velocity. This rock physics property is one of the significantly important parameters for quantitative interpretation due to having positive correlation with thermal conductivity. In this study, we performed seismic inversion to estimate an accurate and high-definition P-wave impedance model using not only reflection data but also refraction data. Moreover, geophysical data integration was done when making a priori model from potential field and elastic wavefield.

For the first step in the seismic inversion process, a priori bulk density model can be calculated by AGG and gravity data and the average density models referring to borehole data. Because we thought that the bulk density model would be much more accurate than a density model inverted from noisy seismic gathers acquired in the mountainous volcanic field. We also take the advantages of refraction tomography giving an accurate P-wave model delineating complex geology at large-scale (Nibe et al., 2018). For the next step, we deal with practical disadvantages regarding spatially limited resolution and sparse ray path coverage in the cost-effective refraction seismic survey. In the workflow, a model-based seismic inversion algorithm is applied for the stacked reflection data after performing routine noise reduction. The model-based inversion scheme starts with a low frequency model of P-impedance, then perturbs a model until a good fit between seismic and synthetic traces. Figure 7 shows vertical cross sections of the bulk density model, the P-wave model derived from refraction tomography and the inverted P-wave impedance model from seismic reflection data, respectively. The multi geophysical data integration allows us to improve the accuracy and resolution of P-wave impedance model for applying to conceptual modelling in the geothermal field in this manner.

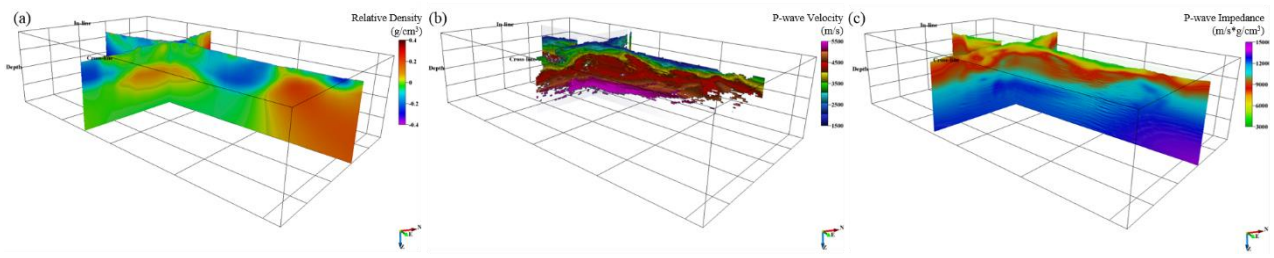

Figure 7: Vertical cross sections of rock property models. (a) The relative density model, (b) the P-wave velocity inverted by refraction tomography and (c) the inverted P-wave impedance model.

4.4.3 Seismic Attributes

In geothermal exploration, there have been published remarkable advances on seismic exploration techniques using refraction and reflection data acquired at volcanic area in Japan (e.g. Fukuda et al., 2017; Mouri et al., 2019). These demonstration projects prove that seismic data is enough quality to carry out both qualitative and quantitative data analysis in geothermal reservoirs. Above all geometric seismic attributes have been contributed to visualization of fractured reservoirs (Chopra and Marfurt, 2007). In oil and gas exploration industry, many algorithms have been developed to automatically and sufficiently detect faults and fractures while removing noise in seismic traces. That is because almost all algorithms are sensitive to random noise. Hence, we applied noise reduction digital filters with a function of dip steering to seismic reflection events. Moreover, reflection events are stretched and distorted in a case of applying inadequate velocity information while time to depth conversion. Therefore, geometric seismic attributes have been popularly extracted in time domain. In this study, we selected different types of geometric attributes consisted of fault likelihood, conventional dip azimuth and curvature attributes for visualization of fault-controlled reservoirs.

First, Hale (2013) defined fault likelihood using a statistical measure of waveform similarity called as semblance. Semblance value is defined by the ratio of the energy of the average data trace to the average energy of each data trace (Roberts, 2001). This fault likelihood is expressed by Equation 1.

$$f \equiv 1 - s^8 \tag{1}$$

where f and s are the fault likelihood and semblance, respectively. Fault likelihood evaluation allows us to quantify the uncertainty of presence of faults and fractures in seismic volume. When applying to seismic reflection data, volumetric scanning can depict statistically thinned fault likelihood (TFL) images associated with faults and fractures. Figure 8 shows an example of TFL attributes in a vertical cross section near the Onikobe power station. Figure 8(Left) illustrates a geological reservoir model based on the drilling well information while Figure 8(Right) shows the seismic section overlaid with TFL attributes. The comparison indicates that TFL attribute can delineate the dominant NW-SE trend faults of the Onikobe caldera.

Secondly, volumetric attributes of dip and azimuth are valuable parameters to evaluate how a given reflector dips in and out of plane of view. The dip vector and strike vector on reflector have been popular seismic attributes in seismic interpretation. These parameters are mathematically calculated by means of complex-trace analysis (e.g. Barnes, 1996; Dalley et al., 1989). Many researches have reported that dip azimuth is one of the geometric attributes to effectively delineate discontinuities associated with large-scale structures and faults. Figure 9 shows a comparison of seismic reflection data, a dip azimuth attribute map, TFL vertical section overlaid with relative density cross section which is jointly inverted from AGG and vertical gravity data. The comparison implies that the dip azimuth attribute can sufficiently delineate the edges of the Onikobe caldera rim and inner structures. Besides, the seismic attribute interpretation is also consistent with that of the inverted relative density model.

Finally, curvature attribute is a morphological measurement defined as the inverse of the radius of a circle that is tangent to a reflection surface at any point (e.g. Roberts, 2001). Several types of curvatures have been introduced for describing relationships between curvature and potential open fractures in reservoir characterization. For example, when assuming two-dimensional reflector is expressed as Equation 2a, most negative and most positive curvatures are minimum and maximum-signed curvatures at any point on quadratic surface, defined as Equation 2b, respectively.

$$\mathrm{z(x,y)} = \mathrm{a}x^2 + cxy + by^2 \tag{2a}$$

$$k_{\pm} = (a+b) \pm [(a-b)^2 + c^2]^{1/2} \tag{2b}$$

where $\mathrm{z(x,y)}$, k_+, k_- are a quadratic surface function of x (inline) axis and y (crossline) axis, most positive and most negative curvatures, respectively. These curvatures are independent of vector dip on reflectors. The attributes can be used to evaluate spatial distributions of faults and associated open fractures for geological structure interpretation (Chopra and Marfurt, 2007). Figure 10 shows a comparison between the gradient of most positive curvature attribute overlaid with resistivity map at 1,200 m depth below MSL, and a seismic cross section overlaid with the TFL attribute. On the resistivity map, there is a boundary at approximately 10 ohm-m which is consistent with the feature of the curvature attribute. The comparison implies that the TFL and curvature attributes can represent faults and fractures that are interpreted by resistivity structure strongly relating to the hydrothermal system in the Onikobe geothermal field. Consequently, it is possible to use these geometric attributes for this conceptual modelling.

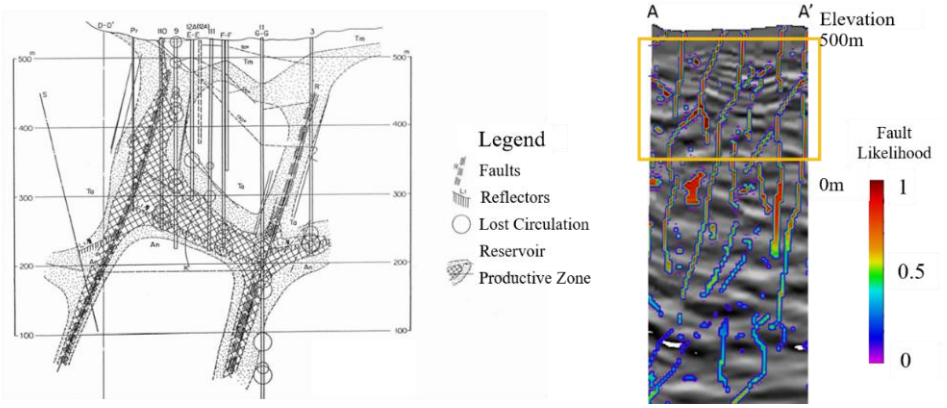

Figure 8: (Left) A geologic cross section (after Abe, 1985), (Right) TFL attribute in the same vertical cross section AA' in depth domain. The square is the coverage of the geologic model.

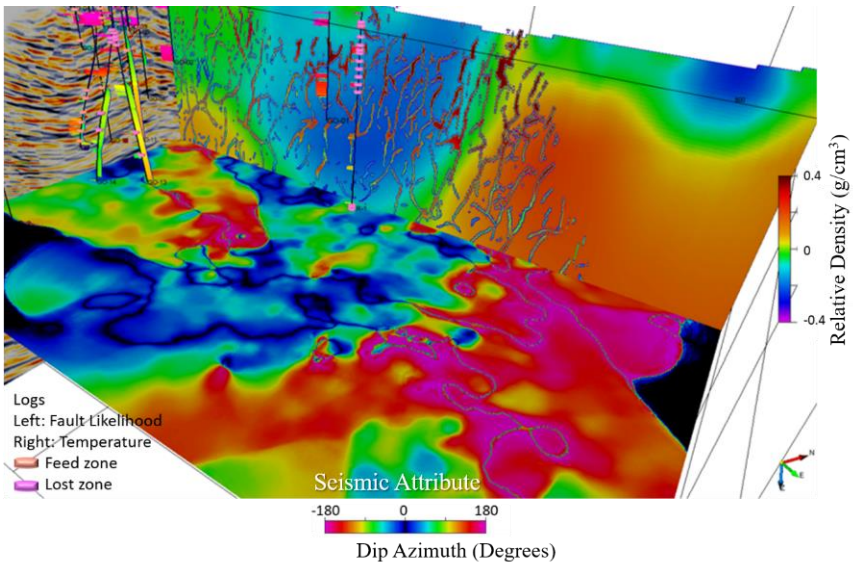

Figure 9: Dip azimuth map at 800 m below MSL, a vertical cross section of TFL overlaid with the relative density jointly inverted from AGG and vertical gravity data, and a seismic section.

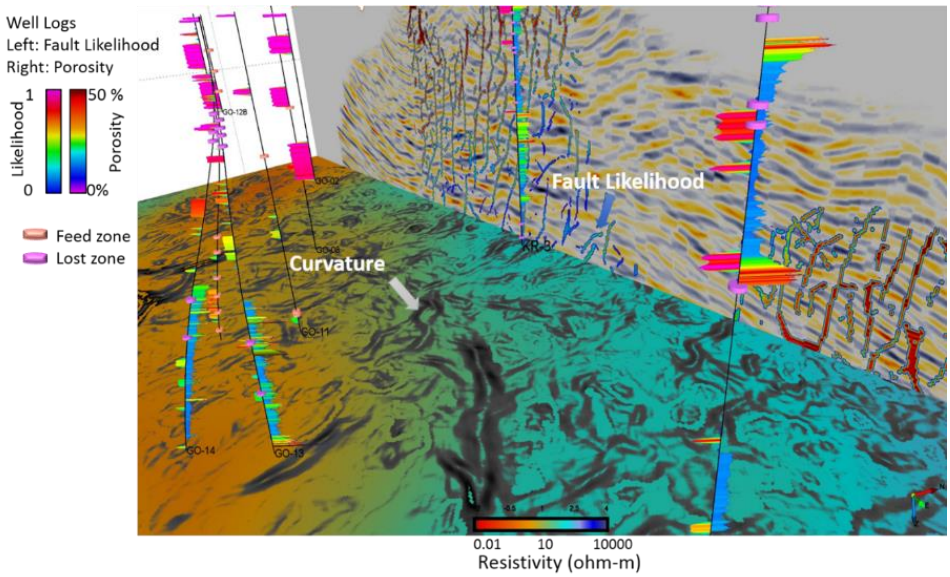

Figure 10: The comparison between the gradient of the most positive curvature attribute overlaid with resistivity map at 1,200 m below MSL, and a seismic section overlaid with TFL. The boundary on the map at approximately 10 ohm-m is consistent with the structure derived from curvature attribute.

5. PROBABLISTIC TEMPERATURE MODELLING

5.1 Methodology

MAA is one of the most frequent used methods for data integration to estimate rock property volumes using seismic data in oil and gas exploration industry. As an application to geothermal industry, Mochinaga et al. (2017) presented a case study to estimate a high-definition temperature based on MAA method using multiple geophysical data and the temperature profiles at well locations. This approach requires a spectral analysis for predicting temperature models at different bandwidths. It assumes that vertical and lateral heat transfer would be caused by different factors in hydrothermal system each other. In fact, long wavelength vertical heat transfer will be caused by convection, conduction and/or radiation from heat source at magma chambers to cooling source at air space. It would be mainly controlled by rock physics properties associated with thermal conductivity. In addition to rock physics properties, in boreholes or casing pipes, outflow and up-flow will form long-wavelength variations in temperature-depth profiles. On the other hand, lateral heat transfer is thought to be caused by high permeability formation and open fractures that are saturated with hydrothermal fluids or groundwater near surface. Thus, feed and lost circulation zones will generate non-linear and short-wavelength variations in temperature-depth profiles. As a machine learning prediction, ANN algorithm has been powerful to estimate short wavelength variations in vertical temperature profiles. In this analysis, short and long wavelength geothermal models are estimated separately. Long wavelength model is set to less than 1 cycle/km and short wavelength model is set to over 2 cycles/km, respectively. After prediction, these two temperature models are merged into a final geothermal model with taper in spatial frequency domain.

5.2 Results

For a final temperature model prediction, we performed the multimodal data integration using the MAA algorithm developed by Hampson et al. (2001). A long wavelength temperature model was predicted by using linear regressions between rock physic

properties and long-wavelength temperature depth profiles at seven trained wells. The functions of input data are mathematically calculated by using a priori temperature model shown in Figure 3, the P-wave impedance model shown in Figure 7(c) and the relative density resistivity model shown in Figure 5. On the other hand, a short wavelength model was predicted by networks between the temperature model, the inverted relative density model, the inverted P-wave velocity model and the seismic attributes described in Section 4.4. Figure 11 shows an example of validation between measured and predicted data of merged temperature profiles at these well locations. The comparison indicates that the approach effectively works to predict the geothermal structure in deeper zones than total depth of wells. Then, each relationship between temperature profiles and the input functions are applied to predict 3D temperature models for short and long wavelengths, respectively. Finally, merging short and long wavelength models makes an accurate and high-definition 3D temperature model. Figure 12 illustrates isothermal surfaces denoting temperatures at 100℃, 200℃ and 300 ℃. A massive heat source is distributed below the power station. The final temperature model is used as a part of criteria for probabilistic conceptual modelling in following sections.

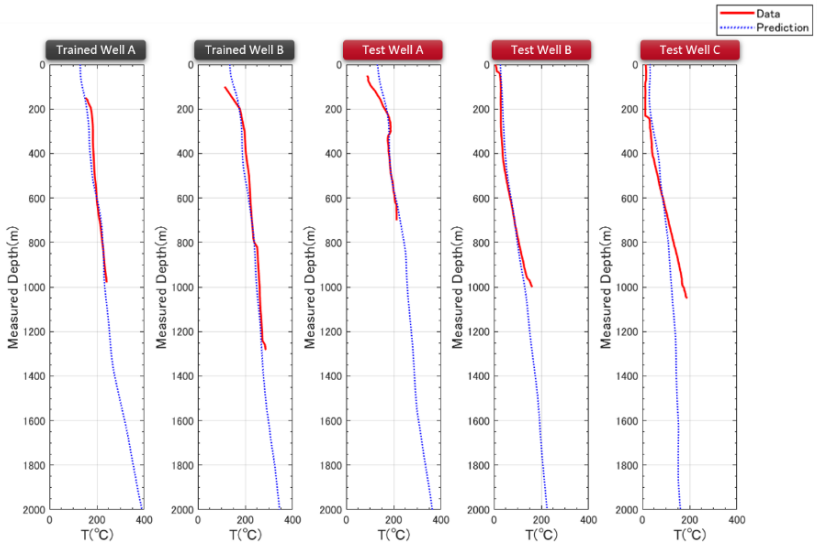

Figure 11: The comparisons between measured (red line) and predicted (dashed blue line) vertical temperature profiles at the trained and test wells.

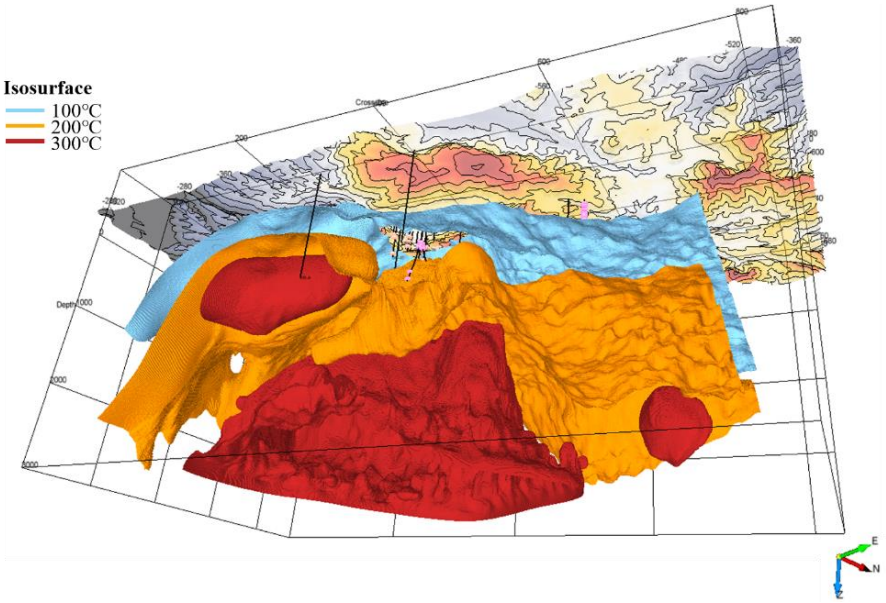

Figure 12: 3D temperature model estimated from the multi-attribute analysis using ANN. Top surface contour map indicates topography.

6. PROBABLISTIC CONCEPTUAL MODELLING

6.1 Resistivity Log Data Analysis

When the litho-facies modelling, it is important to understand which rock physics properties are appropriate to use when classifying both permeable and impermeable zones. For the investigation, at well site, wireline formation tester makes it possible to detect permeability of formation adjacent to borehole. For example, Pressure Temperature and Spinner (PTS) production logging can detect depths of interest in high permeability rocks saturated with high temperature fluids called as feed zones. Besides, mud logging and pressure monitoring system can detect lost circulation zones while drilling. In contrast to these real-time permeability measurement tools, it is necessary to make some assumptions to identify impermeable zones that are associated with hydrothermal system. Mizutani

(2009) analyzed electrical normal logging data to detect impermeable zones, while fluid resistivity and rock porosity estimation beneath the Onikobe caldera. Assuming 100% water saturated rocks, Archie equation is given as Equation 3 (Archie, 1942).

$$R_t = R_w \times a/\phi^m \tag{3}$$

where R_t, R_w, a, ϕ and m are 100% water saturated rock resistivity, formation water resistivity, tortuosity factor, porosity and cementation factor, respectively. With assuming fractured rock case, the constants of a and m were set to 1.0 referring to Mizutani (2009). Then R_t and R_w can be calculated by measurements of resistivity and temperature logging assuming that short normal (SN) measures flushed zone resistivity close to borehole wall and long normal (LN) measures invaded zone resistivity. When pore spaces are saturated with formation water and mud filtrate, the logarithm of the ratio of formation water resistivity to mud filtrate resistivity is expressed as Equation 4.

$$B = \log_{10}(R_w/R_{mf}) \tag{4}$$

where B, R_w and R_{mf} are a constant value, the 100 % water saturated rock resistivity and the mud filtrate resistivity, respectively. The constant of B is calculated by using double logarithmic cross plot of LN and SN data. When pore spaces are replaced by mud filtrate around borehole wall, the change in intercept indicates the change in formation water resistivity. Besides, R_{mf} is set to 80% of observed mud resistivity in the Onikobe field referring to Mizutani (2009). The values of intercept and SN resistivity give the value of R_t in Equation 3. We have investigated impermeable layers from four well locations in the field. Figure 13 shows an example of LN-SN cross plot and the comparison of estimated porosity log data and measured temperature log data at a well location. This cross plot indicates the presence of two types of fluids with different resistivity. We detected the discrepancy of fluid resistivity in approximately 1,000 m depth at the well location. This boundary implies the presence of an impermeable layer in the geothermal system. The analysis makes it possible to compare rock physics properties of permeable and impermeable zones each other.

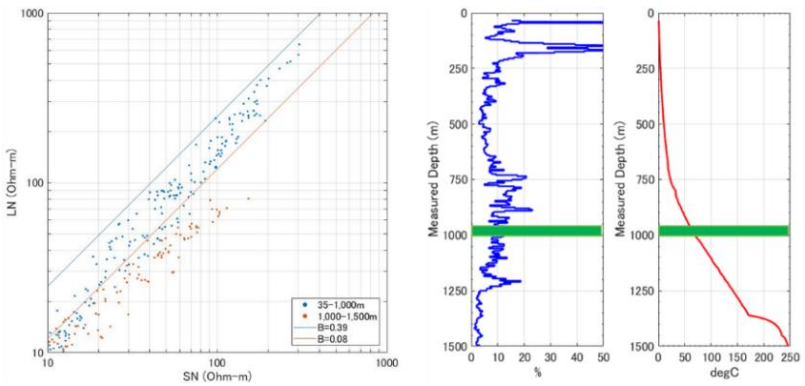

Figure 13: An example of resistivity log data analysis. (Left) A long normal (LN) versus short normal (SN) cross plot, (Center) the estimated porosity and (Right) the temperature log. Green bar indicates a possible impermeable layer on the log data at the borehole location.

6.2 Probability Density

Probability density is one of the well-known and robust approaches to evaluate each facies model uncertainty. Table 1 lists the five facies classification used in our 3D visualization in the Onikobe field. Facies 1 and Facies 2 represent geothermal reservoirs with different temperatures. Facies 3 represents zone with high permeability and low temperature in which candidates of recharge and supplying aquifer in drilling re-injection wells. Facies 4 and Facies 5 represent cap rocks with different clay minerals, respectively. This difference of hydrothermal alteration rocks can be distinguished by temperature criterion. We have investigated the rock physics properties based on this classification. The rock physics properties were examined at observed permeable zones such as feed and lost circulation zones, and at impermeable zones predicted by resistivity log analysis. In addition to wireline logging data, TFL attribute was also investigated in the comparison. Figure 14 illustrates the relationship between P-impedance, resistivity and TFL attribute. It revealed that almost all facies can be distinguished by each probability density distribution using these properties. However, it is difficult to distinguish Facies 1 and Facies 2 according to these distributions. Thus, we applied the final temperature model deterministically as a criterion for separation between two models. As a result, the five facies spatial distributions can be displayed in this conceptual model focusing on temperature and permeability.

Table 1: Facies classification in the demonstration project.

	In-situ Temperature (T)	Permeability (K)	Geology	Concept
Facies 1	T ≥ 190℃	High	Volcanic rocks	Feed zones for flash steam power generation
Facies 2	100℃ ≤ T < 190℃	High	Volcanic rocks	Potential feed zones for binary cycle power generation
Facies 3	T < 100℃	High	Sedimentary and volcanic rocks	Recharge and aquifer zones
Facies 4	T < 150℃	Low	Smectite clay minerals	Cap rocks for the shallow reservoirs
Facies 5	T ≥ 150℃	Low	Pyrophyllite	Cap rocks for the deep reservoirs

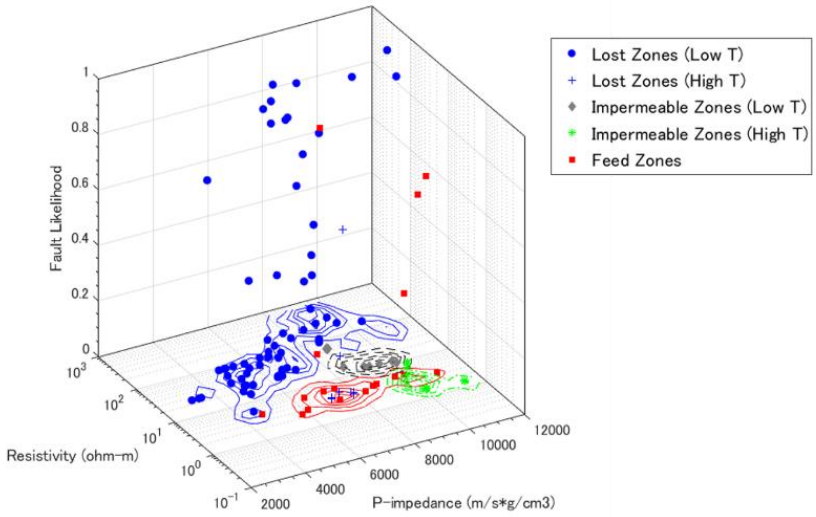

Figure 14: The relationship between permeability, P-impedance, resistivity and TFL attribute. The colored contours indicate PDFs that are calculated by P-wave impedance and resistivity log data.

6.3 Bayesian Classification

We applied a probabilistic classification based on Bayesian posterior estimation theory for the conceptual modelling focusing on permeability and hydrothermal alteration. Bayesian classification is a robust tool to quantify probability distributions of litho-facies uncertainty (e.g. Avseth et al., 2005). Bayesian posterior probability is expressed by Equation 5.

$$p(c_i|X) = \frac{p(X|c_i)p(c_i)}{\sum_{i=1}^{n} p(X|c_i)p(c_i)} \tag{5}$$

where X, c_i, n, $p(c_i|X)$, $p(X|c_i)$, $p(c_i)$, are rock parameters, facies class, the number of facies, the posterior probability of facies class $c_i$given parameter X, the conditional probability of parameter X given the facies class c_i, prior probability of the facies class c_i, respectively. In the calculation, the conditional probability and prior probability of each facies can be evaluated using borehole data. X parameters are three of P-wave impedance, resistivity and TFL attribute. The number n is set to four as described in Section 6.2. Figure 15 illustrates the spatial distribution of high permeability zones implying geothermal reservoirs as defined as Facies 1. There is a cross section of a seismic attribute enhancing the texture of discontinuity on reflectors for improve our understanding. Figure 16 illustrates the spatial distribution of high permeability zones as defined as Facies 3 such as recharge and aquifer area. Figure 17 illustrates the spatial distributions of Facies 4 and Facies 5 representing cap rocks generated by hydrothermal alteration.

Finally, we have performed the comprehensive interpretation based on the comparison of the posteriori probabilities. Figure 18 illustrates the integrated interpretation in the conceptual modelling. The fiver facies models are displayed at the center of the model space, while the final 3D temperature model is displayed at the deep interior of the Onikobe basin. There is a seismic attribute cross section with overlaid the relative density inverted from AGG and vertical gravity data. This comprehensive interpretation has been explicitly delineating the boundary between shallow and deep reservoirs, and the images of faults and fractures.

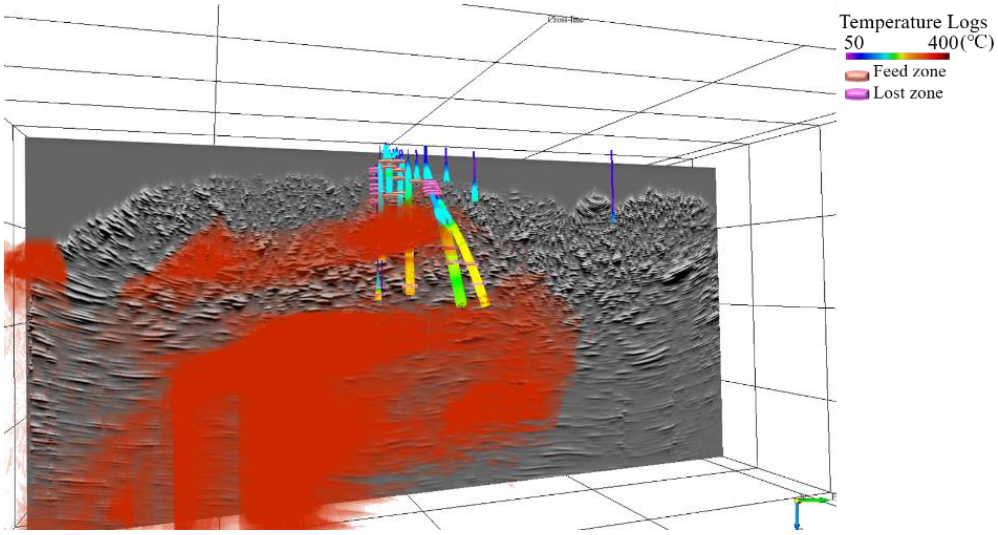

Figure 15**: 3D view of high permeability and high temperature zone defined as Facies 1 in Table 1. A vertical cross section indicates the seismic attribute enhancing discontinuity images on reflectors.**

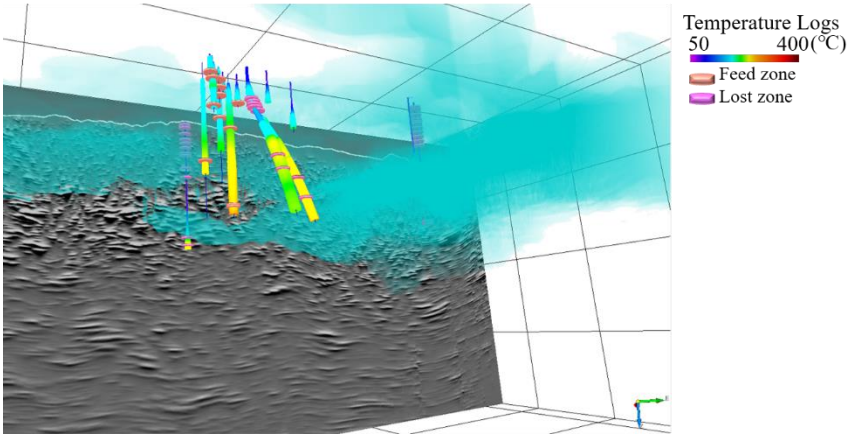

Figure 16: 3D view of high permeability and low temperature zone defined as Facies 3 in Table 1. A vertical cross section indicates the seismic attribute enhancing discontinuity images on reflectors.

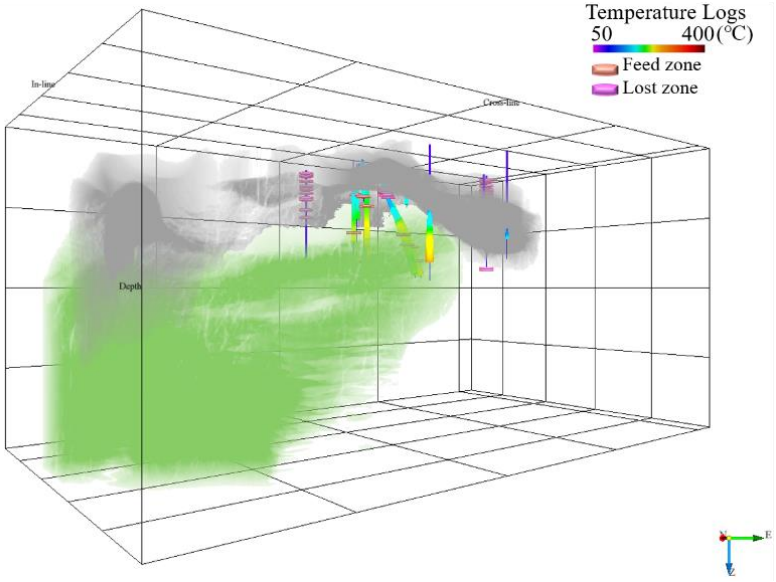

Figure 17: 3D view of impermeable formation models of smectite clay zone (gray) and pyrophyllite altered zone (green) defined as Facies 4 and Facies 5, respectively.

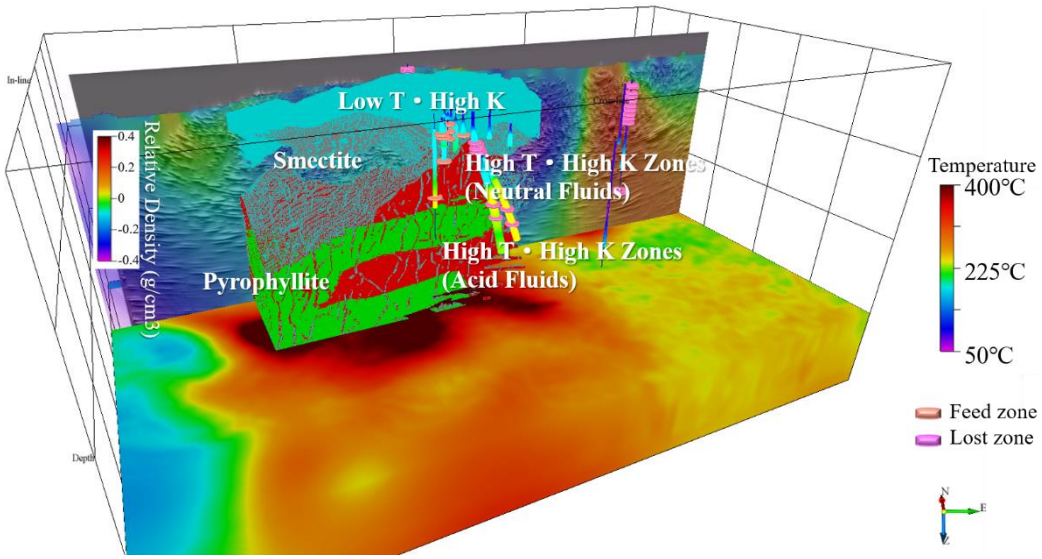

Figure 18: 3D view of the final conceptual model using seismic, MT, AGG, gravity, heat flows and well data. The litho-facies model is located at the center. The bottom of the view shows a part of the final temperature model. The vertical cross section displays the inverted relative density with overlaid the seismic attribute enhancing discontinuity images on reflectors. Temperature log data are displayed with the geologic markers of feed zones (pink) and circulation lost zones (fuchsia) at well locations.

7. CONCLUSION

In this study, the accurate and high-definition conceptual model has revealed the spatial distribution of the impermeable layer which is thought as a boundary between neutral fluids and acid fluids in the Onikobe geothermal field. This probabilistic analysis using multiple geophysical data makes it possible to visualize potential areas representing fractured geothermal reservoir, cap rocks, recharge or aquifer. Besides, the geometric seismic attributes facilitate visualization of the open fractures in the impermeable pyrophyllite rocks. The detailed 3D visualization will achieve better understanding in fluid flow simulation for the next development phase. Consequently, it will allow us to increase the chance of geological success in drilling wells and reduce costs for production sustainability of geothermal resources. Including 3D surface seismic data, multiple geophysical data integration can be a cost-effective geothermal exploration and exploitation from the conceptual model focusing on both temperature and permeability in this manner.

ACKNOWLEDGEMENTS

The authors would like to deeply thank Akasaka, C. and Nakanishi S. of J-Power, Inaba, M., of GeoPuck, and the committees of experts for their continuous supports and valuable suggestions in accomplishment of the JOGMEC demonstration project. We also would like to thank great cooperation of local parties for surface seismic survey at the Onikobe demonstration area.

REFERENCES

Abe, M.: Geothermal Model of the Katayama Field, Onikobe Area (in Japanese with English Abstract), *Journal of the Geothermal Research Society of Japan*, **7** (3), (1985), 283-309.

Archie, G.E.: The Electrical Resistivity Log as an Aid in Determining Some Reservoir Characteristics, *Petroleum Transactions of AIME*. **146**, (1942), 54–62.

Avseth P., Mukerji, T., and Mavko, G.: *Quantitative Seismic Interpretation*, Cambridge University Press, (2005).

Barners, A. E.: Theory of Two-Dimensional Complex Seismic Trace Analysis, *Geophysics*, **61**, (1996), 264-272.

Cai, H. and Zhdanov M. S.: Application of Cauchy-Type Integrals in Developing Effective Methods for Depth-to-Basement Inversion of Gravity and Gravity Gradiometry Data, *Geophysics*, **80**, (2015), G81-G94.

Chopra, S., and Marfurt, K. J.: *Seismic Attributes for Prospect Identification and Reservoir Characterization*, SEG Geophysical Developments, No.11, (2007).

Dalley, R. M., Gevers, E. C. A., Stampfli, G. M., Davies, D. J., Gastaldi, C. N., Ruijtenberg, P. R. and Vermeer D. J.: Dip and Azimuth Displays for 3-D Seismic Interpretation, *First Break*, **7**, (1989).

Endo, M., Zhdanov, M., Gribenko, A., Sunwall, D., Miura, T., Mochinaga, H., Aoki, N. and Mouri, T.: Three-Dimensional Inversion and Interpretation of Multimodal Geophysical Data in Yamagawa Geothermal Field, Japan, *Extended Abstracts*, 80th EAGE Conference and Exhibition (2018).

Fukuda, M., Aoki, N., Satoh, K., Nibe, T., Abe, S., and Tosha, T.: 3D Seismic Survey for Geothermal Reservoir Imaging in the Yamagawa Geothermal Field, Southwestern Japan, *Proceedings*, 38th New Zealand Geothermal Workshop, (2016).

Hale, D.: Methods to Compute Fault Images, Extract Fault Surfaces, and Estimate Fault Throws from 3D Seismic Images, *Geophysics*, **78**, (2013), O33-O43.

Hampson, D. P., Schuelke, J. S., and Quirein, J. A.: Use of Multiattribute Transforms to Predict Log Properties from Seismic Data, *Geophysics*, **66**, (2001), 220-236.

Mizutani, S.: Resistivity Log Analysis of Wells at the Onikobe Geothermal Area, *Annual Meeting Abstract* (in Japanese), the Geothermal Research Society of Japan, (2009).

Mizutani, S.: The Correlation between Seismic and Logging Data and Its Geological Interpretation in the Akinomiya/Wasabizawa Geothermal Area, *Journal of the Geothermal Research Society of Japan*, **34**, (2012), 21-35.

Mochinaga, H., Aoki, N., and Mouri, T.: Advanced 3D Geological Modelling Using Multi Geophysical Data in the Yamagawa Geothermal Field, Japan, *AGU Fall Meeting Abstract*, New Orleans, (2017).

Mouri, T., Aoki, N., Hara, A., Mochinaga, H., Nibe, T., Satoh, K., Kumano, Y., Nakata, M., and Fujiwara, A.: Technical Development for Geothermal Exploration by Seismic Survey and the Second Verification Experiment, *Proceedings*, 44th Workshop on Geothermal Reservoir Engineering Stanford University, (2019).

New Energy and Industrial Technology Development Organization (NEDO): *Report of Investigation on Verification of Geothermal Energy Exploration Technique*, Kurikoma Area (in Japanese), (1985; 1988).

Nibe T., Aoki N. and Mouri, T: Application of 3D Refraction Tomography by Initial Model Randomization and Study on Their Evaluation: Case Study from the Onikobe Quasi-3D Seismic Survey (in Japanese with English Abstract), *Proceedings*, the SEGJ Conference, **138**, (2018), 169-172.

Ogawa, Y., Uchida, T., Sato, I. and Kikuchi, T.: Interpretation of Magnetotelluric Data in the Onikobe Caldera, Northeast Japan, *Rept. Geol. Surv. Japan*, **268**, (1988), 315-331.

Roberts, A.: Curvature Attributes and Their Application to 3D Interpreted Horizons, *First Break*, **19**, (2001), 85-100.

Yamada, E. and Sakaguchi, K.: Geologic Structure Survey in the Onikobe Area. Confirmation Study of the Effectiveness of Prospecting Techniques for Deep Geothermal Resources, Kurikoma Area, *Interim Report of the Sunshine FY1982*, Geol. Surv. Japan, **2**, (1983), 3-36.

Zhdanov, M. S.: *Inverse Theory and Applications in Geophysics*, 2nd ed., Elsevier, (2015).